Small Signal Stability of Fractional Frequency Transmission System With Offshore Wind Farms

Jing Li and Xiao-Ping Zhang, *Senior Member, IEEE*

Abstract—**Fractional frequency transmission system (FFTS) is a relatively new transmission technology that can be used to deliver the energy from remote offshore wind farms, and it can increase the transmission capacity through the reduced transmission frequency. However, the dynamic performance of a FFTS with the wind farm may be different from that of a traditional ac transmission with the wind farm. In this paper, a doubly fed induction generator (DFIG)-based wind farm is connected to the main grid via the FFTS. The detailed dynamic model of the FFTS with wind farm is established first, and then the eigenvalue analysis is carried out to evaluate the system dynamic damping performance. To verify the results of eigenvalue analysis, dynamic simulations are carried out on a single machine infinite bus and a multimachine system. Both eigenvalue analysis and simulations demonstrate that the FFTS will have a negative influence on the damping of the DFIG-based wind farm in comparison to that of the wind farm with the traditional ac transmission system. However, with the control of cycloconverter, this problem can be easily overcome, and the damping performance of wind farm with FFTS can be even better.**

Index Terms—**Cycloconverter, DFIG, Fractional frequency transmission system (FFTS), small signal stability.**

I. INTRODUCTION

WIND energy is considered to be one of the widely used renewable energy sources. The delivery of energy from remote offshore wind farms to the transmission grid becomes a big challenge. To cope with this challenge, a few transmission system schemes have been proposed, such as high voltage alternating current system (HVAC), high voltage direct current system (HVDC) and fractional frequency transmission system (FFTS).

The FFTS [1] is a relatively new option. The concept of FFTS was first proposed in 1994 [1]. It was designed to deliver the hydro-power from the West China to the East China where the transmission distance ranges from 1000 to 2500 km [2]. The objective of FFTS is to increase the transmission system capacity by using lower frequency, e.g. 50/3 Hz [3]. The feasibility of

J. Li was with the Department of Electronic, Electrical, and Computer Engineering, University of Birmingham, Birmingham B15 2TT, U.K. He is now with the State Grid Energy Research Institute, Future Science and Technology Park, Beijing 102209, China (e-mail: jingli0120@163.com).

X.-P. Zhang is with the Department of Electronic, Electrical, and Computer Engineering, University of Birmingham, Birmingham B15 2TT, U.K. (e-mail: x.p.zhang@bham.ac.uk).

FFTS was initially analyzed in [2], and the experimental FFTS was also established to confirm the advantages of FFTS [4]. The core electrical component in a FFTS is the cycloconverter, which is used to convert the low frequency power to the nominal frequency power. Initially, the cycloconverter was used to drive machines in high power applications. The vector control of cycloconverter in machine drives was introduced in [5], [6]. The dynamics of cycloconverter and designed the feedback control for the cycloconverter were presented in [7]. In [8], [9], the application of cycloconverter in the FFTS was studied. Besides, the cycloconverter was also used to control the wind turbines in order to achieve optimal speed control in the FFTS [10].

In case of the offshore wind power transmission, FFTS is more suitable due to the following reasons:

1) As the speed of the wind generation remains in the range from 12 Hz to 18 Hz [10], [11], wind turbine can generate power at this frequency without gearbox [12] or with very small ratio gearbox.

2) Compared with HVAC, the FFTS costs less in long distance transmission considering the investment, maintenance and power losses [3]. Specifically, in the offshore wind transmission, the breakeven distance is not exceeding 50 km via HVAC because of the submarine cable [13].

3) As for HVDC, though it can break through the bottleneck of the transmission distance, it still faces many economical and technical challenges. The power converters at the two ends of HVDC are very expensive and difficult to maintain, especially for the offshore wind farms [13]. In [14], a comprehensive evaluation between FFTS and HVDC was carried out to support the above facts proposed in [13]. In addition, the DC fault management for VSC HVDC system at present is still challenging and expensive.

4) On the other hand, the implementation of FFTS seems to face no special technical difficulty. The key component, cycloconverter, which is used to transform power frequency, is a mature technology [4]. The single phase FFTS have been developed for railway grid in Austria and Switzerland [12]. There is comprehensive industrial knowledge available. Moreover, the FFTS can easily form a network as the conventional AC system does.

In this paper, the FFTS is chosen to deliver the remote offshore wind energy to the main grid. The objectives of this paper are to carry out eigenvalue analysis to investigate the small signal dynamics of such a system; analyze and improve the system damping performance; and use time domain simulations to validate the results.

This paper is organized as follows. In Section II, the principle of FFTS and the structure of the studied systems are

introduced. The detailed mathematical models of the studied systems are depicted in Section III. Section IV conducts the eigenvalue analysis. Section V proposes a feedback control loop on the cycloconverter to improve the damping of the FFTS with wind farms. The time domain simulations are presented in Section VI to verify the results of the eigenvalue analysis and the proposed feedback control.

II. PRINCIPLE AND STRUCTURE

The FFTS, is also referred to as low frequency AC system, is another method to increase the transmission capacity. Fractional frequency or low frequency means the transmission frequency is lower than the nominal one. To make it more clear, the principle of the FFTS will be introduced as follows.

A. Basic Principle

In an AC transmission system, the active power transmitted via the transmission line can be expressed as [15]

$$P = \frac{E_S E_R}{X} \sin \delta \tag{1}$$

where P is the positive power; E_S and E_R are the sending and receiving end voltage, respectively; δ is the transmitting angle; X is the transmission line reactance and it is proportional to the power frequency f,

$$X = 2\pi f L \tag{2}$$

where L is the total inductance of the transmission line.

According to (1), there are two methods to increase the transmission capacity. One is to increase the voltage level, and the other one is to reduce the reactance. The strategy the FFTS adopts is the latter one. Due to the lower frequency, the total reactance of the transmission line in FFTS can be reduced apparently according to (2). This is the basic operating principle of the FFTS.

Besides, the voltage drop of a transmission line can be evaluated by [4]

$$\Delta V\% = \frac{QX}{V^2} \times 100 \tag{3}$$

where Q is the reactive power of the transmission line.

According to the above equation, the voltage drop of the transmission line is proportional to the reactance of the transmission line. So, the voltage fluctuation in the FFTS can be improved.

B. Structure of the Studied Systems

In the studied systems, the offshore wind farm is supposed to be composed of 100 2-MW, 0.69-kV doubly fed induction generator (DFIG)-based wind turbines.

Traditionally, the offshore wind farm generates AC power at nominal frequency (60 Hz), and it is connected to the main grid through a 60 Hz transmission line as Fig. 1 (a).

In this paper, FFTS is proposed to deliver the power generated by the offshore wind farm. The wind farm directly produces 20 Hz (1/3 of 60 Hz) AC power, and the power is delivered through a 20 Hz transmission line. The cycloconverter plays as
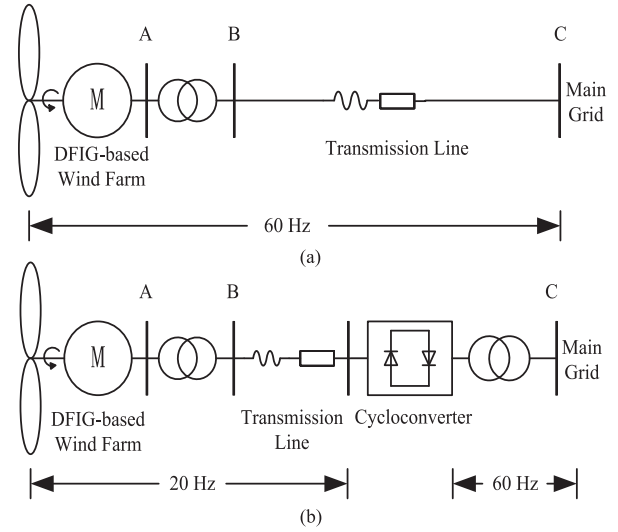

Fig. 1. Configuration of the studied systems. (a) Wind farm with standard AC system (Case 1). (b) Wind farm with FFTS (Case 2).

the interface between the 20 Hz FFTS and the 60 Hz main grid. It can increase the frequency of the power from 20 Hz to 60 Hz. The configuration of the wind farm with FFTS is shown in Fig. 1(b).

For comparison, the following studies are carried out in two cases as presented:

Case 1: the wind farm is directly connected with the main grid through a 100 km 230 kV transmission line, and the transmission frequency is 60 Hz.

Case 2: the wind farm is connected with the low frequency side of cycloconverter through a 100 km 230 kV transmission line, and the frequency of its output power is 20 Hz. The high frequency side of the cycloconverters is linked with the main grid with standard frequency (60 Hz).

III. MODELING OF THE STUDIED SYSTEMS

The major electrical components in Case 1 and 2 include the DFIG-based wind turbines, the transmission line and the cycloconverter. In this section, the mathematical models for these components will be presented separately.

A. DFIG-Based Wind Turbine

In Case 1, the DFIG-based wind turbines generate power at the standard frequency (60 Hz). However, the wind turbines in Case 2 produce power directly at 20 Hz. So, the base frequency of the model for DFIGs in Case 1 and 2 is different. The reduced base frequency in Case 2 may lead to the changes in the model of DFIG-based wind turbine.

The DFIG-based wind turbine is composed of the drive train, the induction machine, the back-to-back converter, the rotor side and grid side converter, as shown in Fig. 2. The mathematical model for each part will be introduced in the following.

1) The Drive Train: The drive train includes the wind turbine, the gearbox, the shafts and other mechanical components, and it is often represented by a two-mass model as shown in
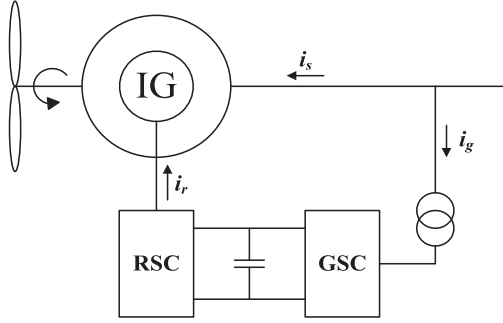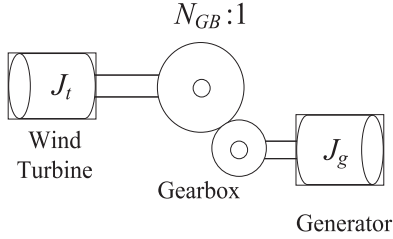
Fig. 2.   Diagram of DFIG-based wind turbine.

Fig. 3.   Two-mass model of drive train.

Fig. 4.   Control block diagram of rotor-side converter.
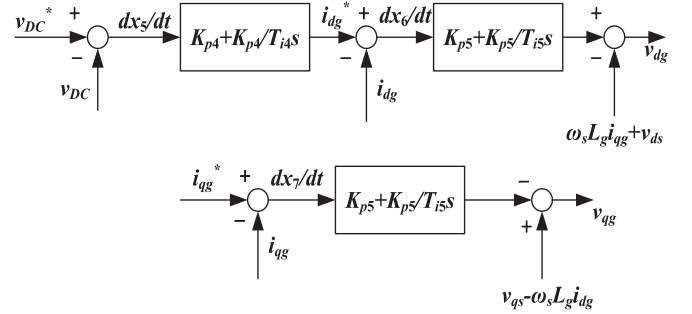
Fig. 5.   Control block diagram of grid-side converter.

Fig. 3. The total moment of inertia of the drive train can be obtained by [16]

$$J = \frac{J_t}{(N_{GB})^2} + J_g \tag{4}$$

where J is the total moment of inertia of the drive train; J_t is the moment of inertia of the wind turbine; J_g is the moment of inertia of the generator; N_{GB} is the gearbox ratio.

Then, the total inertia constant of the drive train can be derived as

$$H = H_t + H_g = J_t \frac{(\omega_b)^2}{2S(N_{GB})^2} + J_g \frac{(\omega_b)^2}{2S} \tag{5}$$

where H is the total inertia constant of drive train; H_t is the inertia constant of the wind turbine; H_g is the inertia constant of the generator; ω_b is the angular velocity of the base frequency; S is the nominal apparent power of the generator.

In Case 2, the DFIGs generate power at 1/3 of the standard frequency, so the base frequency and the gearbox ratio both decrease to 1/3 of those in Case 1. According to (5), as for Case 2, the inertia constant of wind turbine H_t remains the same, and the inertia constant of generator H_g decrease greatly. Consequently, the total inertia constant of the drive train is reduced when the DFIGs are integrated via FFTS.

The mathematical model of the two-mass drive train can be demonstrated as [17]

$$\dot{x}_{wt} = f_{wt}\left(x_{wt}, u_{wt} \right) \tag{6}$$

where $x_{wt} = [\omega_t, \theta_{tw}, \omega_r]^T$, $u_{wt} = [T_e]^T$; ω_t is the angle speed of the wind turbine; ω_r is the angle speed of the rotor of generator; θ_{tw} is the shaft twist angle; T_e is the electromagnetic torque.
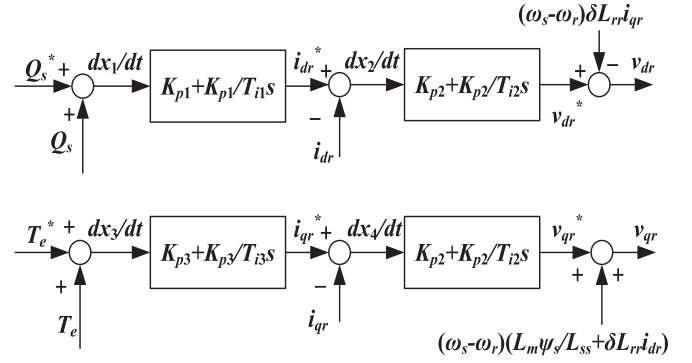
2) Induction Generator: The generator of DFIG is a wound rotor induction machine. The 4th order model of the induction generator, in the *d-q* reference, is given by [17]

$$\dot{\boldsymbol{x}}_g = f_g(\boldsymbol{x}_g, \boldsymbol{z}_g, \boldsymbol{u}) \tag{7}$$

where $\boldsymbol{x}_g = [i_{ds}, i_{qs}, E_d, E_q]^T$, $z_g = [v_{dr}, v_{qr}]^T$, $\boldsymbol{u} = [v_{ds}, v_{qs}]^T$, E'_d and E'_q are the *d* and *q* axis voltages behind the transient reactance, respectively; i_{ds} and i_{qs} are the *d* and *q* axis stator currents, respectively; v_{ds} and v_{qs} are the *d* and *q* axis stator voltages, respectively; v_{dr} and v_{qr} are the *d* and *q* axis rotor voltages.

3) Back-to-Back Converter: The energy is balanced in this converter, so the following equations can be obtained,

$$Cv_{DC} \frac{dv_{DC}}{dt} = v_{dg}i_{dg} + v_{qg}i_{qg} - (v_{dr}i_{dr} + v_{qr}i_{qr}) \tag{8}$$

where v_{dg} and v_{qg} are the *d* and *q* axis voltages of the grid-side converter; i_{dg} and i_{qg} are the *d* and *q* axis currents of the grid-side converter; i_{dr} and i_{qr} are the *d* and *q* axis rotor currents; v_{DC} is the DC capacitor voltage; C is the capacitance of the DC capacitor.

4) Converter Controls: The objective of the rotor side converter is to control the electromagnetic torque and the reactive power of the DFIG. The grid side converter is responsible for maintaining the DC link voltage and controlling the reactive power of the terminal.

The control block diagram of the rotor side converter and grid side converter are shown in Figs. 4 and 5 respectively. x_1, x_2, x_3 and x_4 are the intermediate variables in the controller of rotor
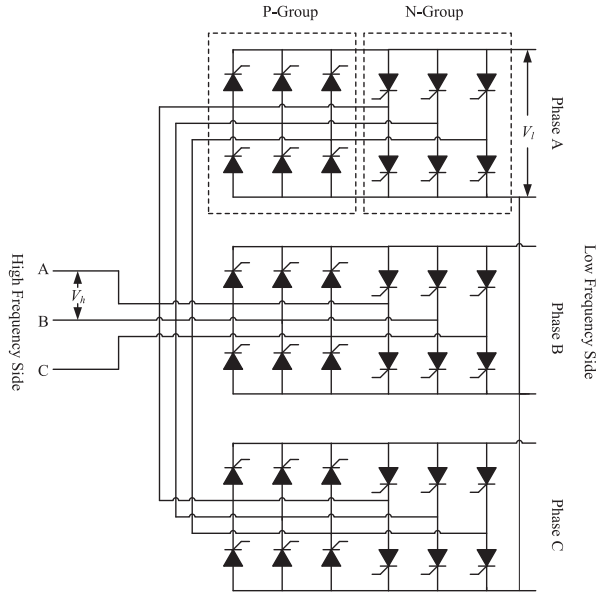
Fig. 6.   Structure of a three phase cycloconverter.

side converter. x_5, x_6 and x_7 are the intermediate variables in the controller of grid side converter.

The entire model (17th order) of a DFIG-based wind turbine can be represented by

$$\dot{\boldsymbol{x}}_{WF} = f(\boldsymbol{x}_{WF}, \boldsymbol{u}) \tag{9}$$

where $x_{WF} = [\boldsymbol{x}_{wt}, \boldsymbol{x}_g, x_1, x_2, x_3, x_4, v_{DC}, x_5, x_6, x_7, i_{dg}, i_{qg}]^T$.

B. Cycloconverter

The cycloconverter is the core component in the FFTS, and it is usually used to drive induction and synchronous motors in high power applications. The structure of a three phase cyclo-converter is shown in Fig. 6, and it consists of 36 thyristors. In each phase, two three phase six-pulse converters, named P-Group and N-Group (also referred to as Positive-Group and Negative-Group), are connected back-to-back.

The cycloconverter was used to step down the frequency of the power in the drive systems. However, in Case 2, the cycloconverter need to step up the transmission frequency from 20 Hz to 60 Hz. This requires both the P-group and N-group in the cycloconverter to operate in their inversion mode. This kind of application was first proposed in [4].

There are two basic operation modes for cycloconverter: circulating current-free mode and circulating current mode. The circulating current mode needs an intergroup reactor to avoid the short circuit, and this increases the size and cost of the cy-cloconverter. As for the circulating current-free mode, although it causes the zero distortion, to some extent, less power losses and higher efficiency can be achieved. In the FFTS, the circu-lating current-free mode is preferred. In this paper, we have the following assumptions.

1) The converter is operated in the non-circulating current mode, or blocking mode.

2) Control algorithm is assumed to be the cosine-wave cross-ing method.

Ideally, the cycloconverter can be modeled as an amplifier with linear gain characteristics. For a 6-pulse cycloconverter with firing angle α [18], the model of cycloconverter can be expressed by

$$V_l = \frac{3\sqrt{2}}{\pi} V_h \cos\alpha \tag{10}$$

$$P_l = P_h \tag{11}$$

$$\cos\theta_h = 0.843 \cos\theta_l \cos\alpha \tag{12}$$

where V_l is the rms value of the line-to-neutral voltage at the low frequency side, V_h is the rms value of the line-to-line voltage at the standard frequency side. θ_h and θ_l are the power factor angle at the standard frequency side and the low frequency side, respectively.

However, the practical cycloconverter is a discrete-time sys-tem, and the control voltage of the cycloconveter is sampled periodically. During the sampling period, the control voltage may step up or down, and this lead to the uncontrolled time of the thyristors in a cycloconverter [7]. The uncontrolled time is often modeled as a time delay element. For more practical modeling of cycloconverter, the (10) can be rewritten as

$$V_l = \frac{3\sqrt{2}}{\pi} V_h \cos\alpha \bullet 1(t - T_s) \tag{13}$$

where T_s is the uncontrolled time of the thyristors. The value of the uncontrolled time is random, and its average value can be approximated by

$$T_s = \frac{1}{2mf_1} \tag{14}$$

where f_1 is the frequency of the standard power, and m is pulse number of a commutation cycle.

The Laplace transform of (13) can be obtained as

$$V_l(s) = \frac{3\sqrt{2}}{\pi} V_h e^{-T_s s} \cos\alpha. \tag{15}$$

The time delay can also be expressed by

$$e^{T_s s} = 1 + T_s s + \frac{1}{2!} T_s^2 s^2 + \frac{1}{3!} T_s^3 s^3 + \cdots. \tag{16}$$

Ignoring the high order terms in (16), (15) can be treated approximately as

$$V_l(s) = \frac{3\sqrt{2}}{\pi} V_h \frac{\cos\alpha}{1 + T_s s}. \tag{17}$$

In the time domain, the above equation is transformed as

$$\frac{dV_l}{dt} = -\frac{V_l}{T_s} + \frac{3\sqrt{2}}{\pi T_s} V_h \cos\alpha. \tag{18}$$

TABLE I
SELECTED EIGENVALUES OF DFIG-BASED WIND FARM
WITH FFTS AND STANDARD AC SYSTEM

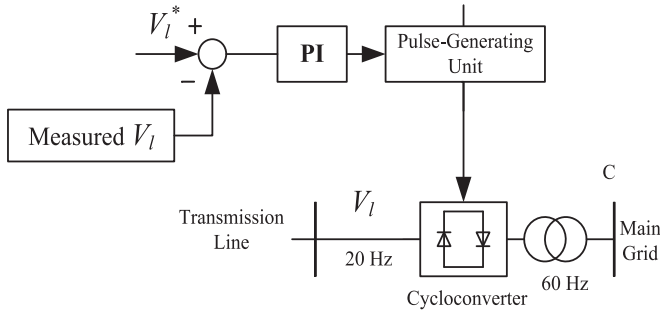| Dominant States	Case 1(60 Hz)	Damping	Case 2(20 Hz)	Damping
i_{ds}, i_{qs}	$-79.54 \pm 383.67i$	20.30%	$-26.50 \pm 193.22i$	13.60%
i_{dg}, i_{qg}	$-1.35 \pm 377.30i$	0.36%	$-0.03 \pm 128.16i$	0.02%
E'_d, E'_q	$-4.56 \pm 17.66i$	25.00%	$-0.70 \pm 13.11i$	5.33%
ω_r	$-6.05 \pm 18.58i$	31.00%	$-2.41 \pm 13.58i$	17.10%
v_{DC}	$-1.09 \pm 7.49i$	14.40%	$-0.16 \pm 4.40i$	3.63%

Fig. 7.   Feedback control loop for cycloconverter.

C. Transmission Line

In the d-q referencew frame, the voltage equation of the transmission line is given by

$$\begin{bmatrix} v_{ds} \\ v_{qs} \end{bmatrix} = \begin{bmatrix} \cos(\varphi_1 - \varphi_2) \\ -\sin(\varphi_1 - \varphi_2) \end{bmatrix} V_l - \begin{bmatrix} R_{TL} & -X_{TL} \\ X_{TL} & R_{TL} \end{bmatrix}$$
$$\times \left(\begin{bmatrix} i_{ds} \\ i_{qs} \end{bmatrix} + \begin{bmatrix} i_{dg} \\ i_{qg} \end{bmatrix} \right) \qquad (19)$$

where $V_s \angle \varphi_1$ is the voltage angle of the DFIG; $V_l \angle \varphi_2$ is the voltage angle at the low frequency side of the cycloconverter; X_{TL} is the combined reactance of the transmission line and the transformer; R_{TL} is the combined resistance of the transmission line and the transformer.

IV. EIGENVALUE ANALYSIS

For the sake of simplicity, the main grid in Case 1 and Case 2 are supposed to be the infinite bus in the following eigenvalue analysis. The state space model of the DFIG-based wind farm are derived from (9) at a steady state operating point. It can be written by

$$\Delta \dot{x}_{WF} = A_{WF} \Delta x_{WF} + B_{WF} \Delta u. \qquad (20)$$

The linearized equation of cycloconverter can be derived from equation (18) as

$$\Delta \dot{x}_{cyc} = A_{cyc} \Delta x_{cyc}. \qquad (21)$$

According to (19), the linearized equation of the transmission line can be expressed in an algebraic equation as

$$\Delta u = C_1 \Delta x_{WF} + C_2 \Delta x_{cyc}. \qquad (22)$$

The inputs in (20) can be eliminated by (22). Then, the model of the Case 2 can be represented by a complete state space equation as

$$\Delta \dot{x} = A \Delta x \qquad (23)$$

where $\Delta x = [\Delta x_{WF}, \Delta x_{cyc}]^T$.

The model for Case 1 can also be obtained by excluding the state of cycloconverter in (23).

The eigenvalue analysis of both Case 1 and Case 2 are carried out. The wind speed is supposed to be 12 m/s, and the output power of each DFIG is 2 MW. The wind farm is obtained by aggregating 100 2-MW DFIG into an equivalent DFIG, and the parameters of a single DFIG are given in the Appendix.

The eigenvalues of the wind farm in Case 1 and Case 2 are shown in Table I. Compared with Case 1, the damping of wind farm in Case 2 decreases significantly. This means the FFTS has a negatively effect on the damping of DFIG-based wind farm.

The reduced damping of FFTS with the wind farm is mainly attributed to the reduced inertia constant of the drive train in DFIG. Based on previous model analysis, the major difference of the DFIG model in Case 1 and Case 2 is the transmission frequency. According to (5), if the transmission frequency is 1/3 of the standard frequency in the FFTS, the total inertia constant of the drive train in DFIG is reduced obviously. The reduced inertia constant finally leads to less damping of the FFTS with wind farms.

V. DYNAMIC DAMPING IMPROVEMENTS FOR FFTS

From the analysis in the previous section, it is found that the FFTS decreases the damping of DFIG-based wind farm obviously. To improve the damping performance of wind farms, the damping controller [19] and better control design [17] for DFIG are two established approaches. However, these approaches are based on the model of a single or a single aggregated DFIG. In fact, the DFIGs in a wind farm usually operate at different operating points. Thus, the general effectiveness of these two methods needs further discussion.

In this paper, this problem can be easily solved by adding additional control loop to improve the damping of FFTS. In the FFTS, the cycloconverter is a thyristor phase-controlled converter, and it is possible to devise a feedback control loop on it to improve the damping of FFTS. Through the feedback control on the cycloconverter, the dynamic performance of the whole wind farm can be manipulated, no matter with the operating point of individual DFIG. In the following section, the general effectiveness of this controller will be verified through the simulations in both the single DFIG system and the multiple DFIGs system.

As mentioned before in this paper, the cycloconverter applies cosine-wave crossing method, which is an open-loop control. This method generates firing instants for the cycloconverter in a fixed procedure. To improve the situation, a feedback control loop is proposed shown as Fig. 7. The voltage of the low frequency side of cycloconverter V_1 is chosen as the feedback signal, and the proportional-integral controller is used to tune the control reference.
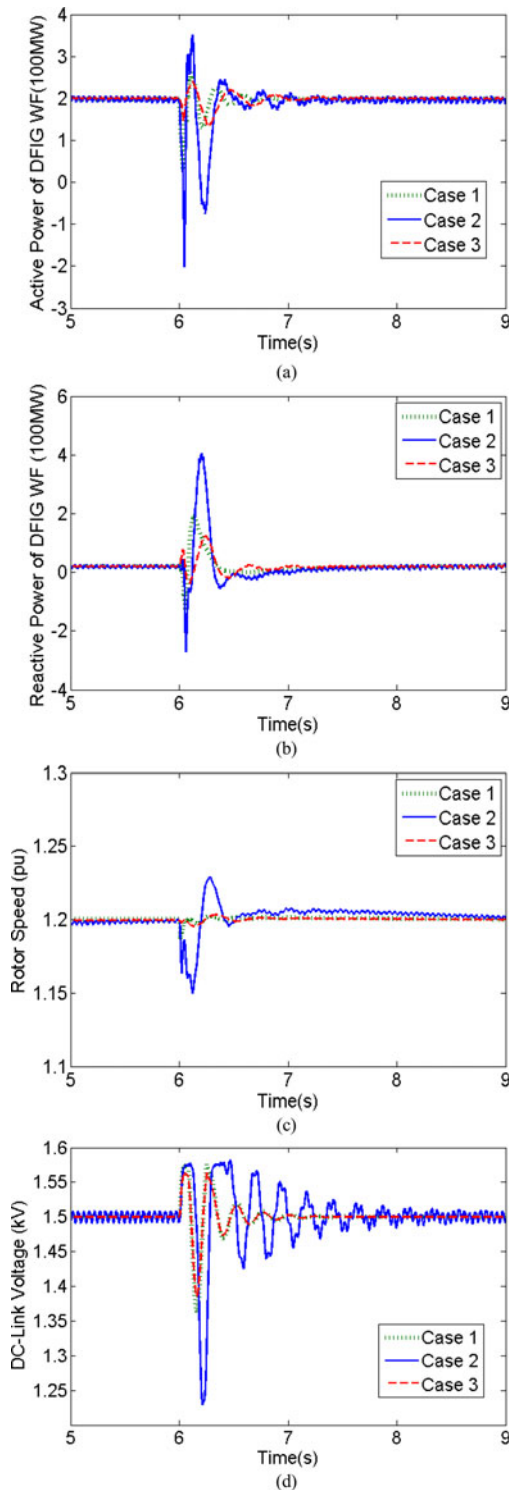
Fig. 8.   Dynamic responses of wind farm for Case 1, 2, and 3 under fault.

To verify the effectiveness, the proposed control loop is implemented in the FFTS in the following simulations. It is tested in both SMIB and multi-machine system.

VI. Dynamic Simulations

To verify the results of eigenvalue analysis and the proposed controller, the dynamic simulations are carried out in
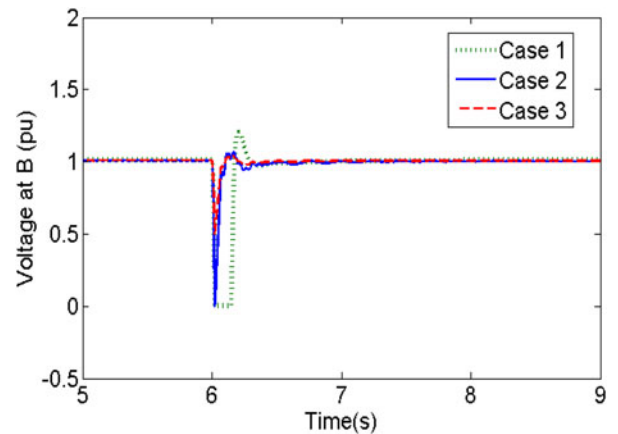

Fig. 9.   Voltage profile at Bus B for Case 1, 2, and 3 under fault.

PSCAD/EMTDC. The following simulations are conducted in a single machine infinite bus (SMIB) and a multi-machine system, respectively. The dynamic responses are compared between the FFTS with wind farms and the conventional AC system with wind farms.

A. Simulations on SMIB System

In this part, the wind farm is obtained by aggregating 100 2-MW DFIG into an equivalent DFIG. The simulations are carried out in SMIB to observe the dynamic responses in the following three cases:

Case 1 and *Case 2:* as described in Section II. The main grid is substituted by an infinite bus.

Case 3: a control feedback loop is added to cycloconverter in the FFTS with DFIG-based wind farm (Case 2).

1) Dynamic Responses Against Disturbances: In order to study the dynamics of Case 1 and Case 2, a three-phase ground fault is applied to excite the corresponding dynamic responses. The three-phase ground fault happens at Bus Bin both cases as shown in Fig. 1. It starts at 6.0 s during the simulation, and then it is cleared after 0.025 s.

Fig. 8 shows the dynamic responses of the active power, reactive power, rotor speed, DC-link voltage of the DFIG in Case 1 and Case 2. From the dynamic responses, it can be concluded that the damping of the wind farm with the FFTS decrease significantly compared with the wind farm with conventional AC system.

Fig. 9 shows the voltage profile at Bus B after the fault. In the FFTS, the voltage fluctuation at Bus B is improved compared with that in the standard AC system. According to (3), the improved voltage fluctuation is attributed to the reduced reactance of the transmission line in the FFTS.

2) Damping Improvement for FFTS: From previous simulations, it is observed that the FFTS reduces the damping of wind farms significantly compared with standard AC system. To improve the damping of FFTS, an additional feedback control loop on cycloconverter is proposed as Fig. 7, and its effectiveness is also verified through the simulations in SMIB. The same fault in Case 1 and Case 2 is also applied in Case 3.
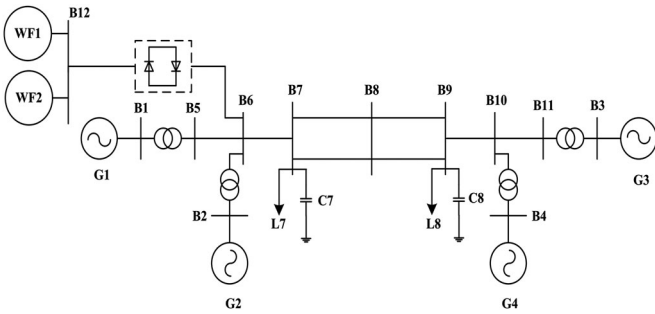
Fig. 10.   Configuration of the simulations in four-machine system.

Fig. 8 compares the dynamic responses of the active power, reactive power, rotor speed, DC-link voltage in Case 3 with those in Case 1 and Case 2. With the support from additional controller on cycloconverter, the damping of the wind farm with FFTS is greatly improved, and it can be even better than the wind farm with standard AC system. The simulation results also indicate that the problem of less damping in the FFTS can be easily solved by adding feedback control loop.

Fig. 9 compares the voltage at Bus B in Case 3 with those in Case 1 and 2. The voltage fluctuation can be further improved with the additional controller on the cycloconverter.

B. Simulations on Multi-Machine System

To further verify the general effectiveness of the small signal analysis and the proposed controller, the simulations will be conducted in the four-machine system. The four-machine system is shown as Fig. 10, and the details of system can be found in [15].

Moreover, the wind farm in previous section is divided into two wind farms: WF1 and WF2. Each wind farm includes 50 DFIG, but the wind speed is different for each one. The wind speed for WF1 is 10.903 m/s, and the output power for a single DFIG is 1.5 MW. The WF2 is under 12 m/s wind speed, and the output power for a DFIG is 2 MW.

For comparison, simulations are carried out in the following three cases:

Case 4: the WF1 and WF2 are directly connected to B6 (as in Fig. 10) through a 100 km 230 kV standard AC transmission line.

Case 5: the WF1 and WF2 are integrated with the four-machine system through a 100 km 230 kV low frequency transmission line. The low frequency side of the cycloconverter is connected to B12, and the high frequency side is linked with B6 in the four-machine system.

Case 6: based on Case 5, the proposed controller is implemented on cycloconverter as shown in Fig. 7.

In Case 4, 5 and 6, the total output power of WF1 and WF2 is 175 MW. Consequently, the output of G1 is reduced by 175 MW to guarantee the overall output from G1 and wind farm remain 900 MW.

1) Dynamic Responses Against Disturbances: The three-phase ground fault happens at B8 as shown in Fig. 9. It starts at 6.0 s in both Case 4 and Case 5, and then it is cleared after 0.1 s.
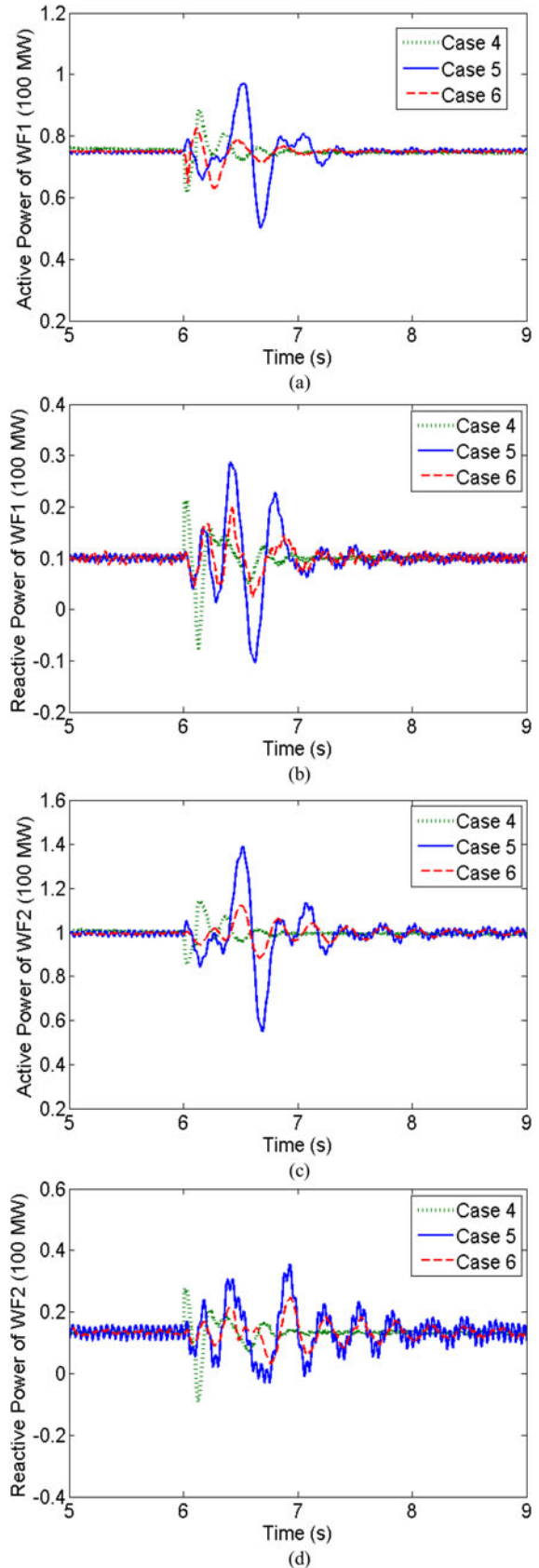

Fig. 11.   Dynamic responses of WF1 and WF2 for Case 4, 5, and 6 under fault.

TABLE II
EIGENVALUES OF DFIG-BASED WIND FARMS IN CASE 4 AND CASE 5

| Dominant States	Case 4 (60 Hz)	Damping	Case 5 (20 Hz)	Damping
i_{ds}, i_{qs} (WF1)	$-61.60 \pm 377.84i$	16.10%	$-24.10 \pm 168.52i$	14.20%
i_{dg}, i_{qg} (WF1)	$-5.06 \pm 375.79i$	1.35%	$-0.8 \pm 125.23i$	0.64%
E_d', E_q' (WF1)	$-6.90 \pm 33.89i$	20.00%	$-1.83 \pm 19.48i$	9.35%
ω_r (WF1)	$-2.87 \pm 16.58i$	17.10%	$-0.97 \pm 9.67i$	9.98%
v_{DC} (WF1)	$-1.64 \pm 7.93i$	20.30%	$-0.29 \pm 5.18i$	5.59%
i_{ds}, i_{qs} (WF2)	$-39.10 \pm 377.84i$	10.30%	$-13.90 \pm 168.52i$	8.22%
i_{dg}, i_{qg} (WF2)	$-5.04 \pm 375.77i$	1.34%	$-0.75 \pm 125.24i$	0.60%
E_d', E_q' (WF2)	$-6.94 \pm 33.92i$	20.00%	$-1.84 \pm 19.46i$	9.41%
ω_r (WF2)	$-2.87 \pm 16.59i$	17.00%	$-0.96 \pm 9.67i$	9.88%
v_{DC} (WF2)	$-1.77 \pm 8.89i$	19.5%	$-1.04 \pm 5.78i$	17.70%
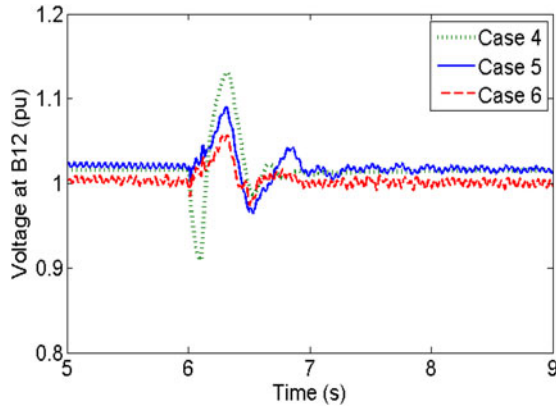
Fig. 12. Voltage profile at Bus B12 for Case 4, 5, and 6 under fault.

Fig. 11 demonstrates the dynamic responses of the active power and reactive power in both WF1 and WF2 for Case 4 and Case 5. The state responses in the four-machine system also indicate that the damping of the DFIG-based wind farm with the FFTS decrease significantly compared with that of the wind farm with traditional AC system, which is the same as the simulation results in SMIB. The eigenvalues of the wind farms in Case 4 and Case 5, as shown in Table II, also confirm the above result.

Fig. 12 shows the voltage profile at Bus B12 in Case 4 and Case 5, and it also indicates that the voltage response is improved in the FFTS.

2) Damping Improvement for FFTS: The effectiveness of the proposed controller on the cycloconverter is also tested in the four-machine system.

Fig. 11 shows the dynamic responses of the active and reactive power in both WF1 and WF2 in Case 6. From the dynamic responses of Case 6, the cycloconverter with additional control can greatly improve the damping of the wind farm with FFTS. Meanwhile, with the help of cycloconverter, the damping of wind farm with FFTS can perform better than that of the wind farm with the traditional AC transmission system.

Fig. 12 demonstrates that the feedback controller on the cycloconverter can further improve voltage fluctuation at Bus B12.

VII. CONCLUSION

This paper has applied the FFTS to deliver the power generated by a DFIG-based offshore wind farm to the main transmission grid. The mathematical model of the FFTS has been proposed in detail. Based on the model established, eigenvalue analysis has been conducted to investigate the dynamics of the DFIG-based wind farm with FFTS. The time domain simulations have also been conducted in the SMIB and four-machine system to verify the results of the eigenvalue analysis. Both eigenvalue analysis and time domain simulations have demonstrated that the damping of the DFIG-based wind farm is greatly decreased by utilizing the FFTS in comparison with the wind farm with the traditional AC transmission system. However, this problem can be easily overcome by adding control loop to the cycloconverter. With the control loop, the damping of the wind farm with FFTS can perform better than that of the wind farm with with traditional AC system.

APPENDIX

A. Data of the DFIG-Based Wind Turbine

1) Per unit system: $S_b = 2.2$ MW, $V_b = 0.69$ kV.
2) Wind Turbine: $V_w = 12$ m/s, $C_p = 0.4382$, $R = 37.049$ m, $\rho = 1.225$ kg/m^3, $H_t = 1$ s.
3) The generator of DFIG:

$$R_s = 0.00462 \text{ pu}, L_m = 4.348 \text{ pu}, L_{ss} = 4.450 \text{ pu},$$

$$L_{rr} = 4.459 \text{ pu}, R_r = 0.006007 \text{ pu}, H_g = 0.5 \text{ s}.$$

4) Converter: $C = 0.11$F, $v_{DC} = 1.5$ kV, $L_g = 0.3$ pu, $R_g = 0.003$ pu.
5) Control parameter: $K_{p1} = 0.5, T_{i1} = 0.4, K_{p2} = 0.025, T_{i2} = 0.075, K_{p3} = 0.5, T_{i3} = 0.4, K_{p4} = 1, T_{i4} = 0.05, K_{p5} = 0.8, T_{i5} = 0.032$.

B. Data of the Transmission Line

Length of the transmission line: 100 km
Line-to-line RMS voltage: 230 kV
Combined resistance of the transformer and transmission line: $R_{TL} = 5\,\Omega$
Combined inductance of the transformer and transmission line: $L_{TL} = 0.13$ H

C. Parameters of the Controller on Cycloconverter

$K_p = 100, \ T_i = 0.01$

REFERENCES

[1] X. Wang, "The fractional frequency transmission system," in *Proc. IEEE Jpn. Power Energy*, Tokyo, Japan, Jul. 1994, pp. 53–58.
[2] X. Wang and X. Wang, "Feasibility study of fractional transmission system," *IEEE Trans. Power Syst.*, vol. 11, no. 2, pp. 962–967, May 1996.
[3] X. Wang, X. Wang, and Y. Teng, "Fractional frequency transmission system and its application," *Proc. CSEE*, vol. 32, no. 13, pp. 1–6, May 2012.
[4] X. Wang, C. Cao, and Z. Zhou, "Experiment on fractional frequency transmission system," *IEEE Trans. Power Syst.*, vol. 21, no. 1, pp. 372–377, Feb. 2006.

[5] B. K. Bose, *Modern Power Electronics and AC Drives*. Englewood Cliffs, NJ, USA: Prentice-Hall, 2002.

[6] S. P. Da and A. K. Chattopadhyay, "Observer-based stator-flux-oriented vector control of cycloconverter-fed synchronous motor drive," *IEEE Trans. Ind. Appl.*, vol. 33, no. 4, pp. 943–955, Jul./Aug. 1997.

[7] W. Hill, E. Ho, and I. Neuzil, "Dynamic behaviour of a cycloconverter system," in *Proc. IEEE Ind. Appl. Soc. Annu. Meet.*, 1990, pp. 1024–1030.

[8] Y. Cho, G. J. Cokkinides, and A. P. Meliopoulos, "Time domain simulation of a three-phase cycloconverter for LFAC transmission systems," in *Proc. Power Energy Soc. Trans. Distrib. Conf. Exhib.*, Orlando, FL, USA, May 2012, pp. 1–7.

[9] Y. Teng and X. Wang, "Three-phase short-circuit fault on the lower frequency bus of cycloconverter in FFTS," in *Proc. Power Syst. Conf. Expo.*, 2009, pp. 1–5.

[10] Z. Song, X. Wang, Y. Teng, L. Ning, and Y. Meng, "Optimal control study for fractional frequency wind power system," in *Proc. Asia-Pacific Power Energy Eng. Conf.*, 2012, pp. 1–5.

[11] L. Ning, X. Wang, and Y. Teng, "Experiment on wind power grid integration via fractional frequency transmission system: Realization of the variable-speed variable-frequency power wind," in *Proc. 4th Int. Conf. Electr. Utility Deregulation Restruct. Power Technol.*, Jul. 2011, pp. 444–449.

[12] W. Fischer, R. Braun, and I. Erlich, "Low frequency high voltage offshore grid for transmission of renewable power," in *Proc. IEEE 3rd PES Innovative Smart Grid Technol. Eur.*, Berlin, Germany, 2012, pp. 1–6.

[13] Q. Nan, Y. Shi, X. Zhao, and A. Vladislav, "Offshore wind farm connection with low frequency AC transmission technology," in *Proc. Power Energy Soc. General Meet.*, 2009, pp. 1–8.

[14] S. A. P. Meliopoulos, D. Aliprantis, Y. Cho, D. Zhao, A. Keeli, and H. Chen, "Low frequency transmission," *Final Project Report*, PSERC Publication 12-28, Oct. 2012, Power Systems Engineering Research Center, Arizona State Univ., 527 Engineering Research Center, Tempe, AZ, USA.

[15] P. Kundur, *Power System Stability and Control*. New York, NY, USA: McGraw-Hill, 1994.

[16] S.M. Muyeen, M. H. Ali, R. Takahashi, T. Murata, J. Tamura, Y. Tomaki, A. Sakahara, and E. Sasano, "Comparative study on transient stability analysis of wind turbine generator system using different drive train models," *IET Renewable Power Generation*. vol. 1, no. 2, pp. 131–141, 2007.

[17] F. Wu, X.-P. Zhang, K. Godfrey, and P. Ju, "Small signal stability analysis and optimal control of a wind turbine with doubly fed induction generator," *IET Generation Transmiss. Distrib.* vol. 1, no. 5, pp. 751–760, Sep. 2007.

[18] B. R. Pelly, *Thyristor Phase-Controlled Converters and Cycloconverters*. New York, NY, USA: Wiley, 1971.

[19] Y. Mishra, S. Mishra, M. Tripathy, N. Senroy, and Z. Y. Dong, "Improving stability of a DFIG-based wind power system with tuned damping controller," *IEEE Trans. Power Syst.*, vol. 24, no. 3, pp. 650–660, Sep. 2009.

Jing Li received the B.Eng. degree from Chongqing University, Chongqing, China, and the M.Eng. degree from the University of Science and Technology of China, Hefei, China, in 2009 and 2012, respectively. He obtained the Ph.D degree in electrical engineering from the University of Birmingham, Birmingham, U.K. in 2016. He is now with the Department of Corporate Strategy Research, State Grid Energy Research Institute.

Xiao-Ping Zhang (M'95–SM'06) received the B.Eng., M.Sc., and Ph.D. degrees in electrical engineering from Southeast University, Nanjing, China, in 1988, 1990, 1993, respectively. He is currently a Professor of electrical power systems at the University of Birmingham, Birmingham, U.K. He is also the Director of Smart Grid, Birmingham Energy Institute and the Co-Director of Birmingham Energy Storage Centre. Before joining the University of Birmingham, he was an Associate Professor at the University of Warwick, England, U.K. From 1998 to 1999, he was visiting UMIST. From 1999 to 2000, he was an Alexander-von-Humboldt Research Fellow with the University of Dortmund, Germany. Between 1993 and 1998, he worked at the China State Grid EPRI (NARI Group) on EMS/DMS advanced application software research and development. He is the co-author of the 1st and 2nd edition of the monograph "*Flexible AC Transmission Systems: Modeling and Control,*" (Springer, 2006, 2012) and "*Restructured Electric Power Systems: Analysis of Electricity Markets with Equilibrium Models,*" (IEEE Press/Wiley, 2010). Internationally, he pioneered the concept of "Energy Union" and "UK's Energy Valley."